Hindawi
Mathematical Problems in Engineering
Volume 2020, Article ID 4163206, 11 pages
https://doi.org/10.1155/2020/4163206

Research Article

Experimental Investigation of Thermal Conductivity and Specific Heat of the Calcium Phosphate Ore for a Drying Application

Zhor El Hallaoui,[1,2] **T. Moudakkar**,[1,2] **S. Vaudreuil**,[2] **T. Bounahmidi**,[2] **and S. Abderafi**[1]

[1]*Laboratoire D'Analyse et Synthèse des Procédés Industriels, Ecole Mohammadia D'Ingénieurs, Université Mohamed V, Rabat, Morocco*
[2]*Euromed Research Institute, Euro-Mediterranean University of Fes, Fes, Morocco*

Correspondence should be addressed to Zhor El Hallaoui; zhor.hallaoui@gmail.com

Received 14 July 2020; Revised 30 August 2020; Accepted 30 September 2020; Published 26 October 2020

Academic Editor: Francisco R. Villatoro

This paper discusses an experimental investigation to determine regression models for thermal properties of phosphate particles and to analyze the performances of the phosphate flash dryer. For this purpose, the specific heat capacity and thermal conductivity of phosphate particles were experimentally determined by the modulated differential scanning calorimetry (MDSC) and the modified transient plane source method (MTPS), respectively. Multiple regression models were developed to correlate the specific heat and thermal conductivity to moisture content, particle size, and temperature. Experimental results showed that the measured thermal conductivity and dry specific heat were found in the range of 0.07–0.61 W/m K and 510–630 J/kg·K, respectively. Furthermore, the specific heat increased almost linearly with temperature but decreased with particle size, while the thermal conductivity increased with moisture content and temperature but decreased with particle size. These correlations were integrated to the phosphate flash dryer mathematical model and used to analyze the thermal behavior of phosphate drying. Simulation results were compared to experimental data obtained on a bench-scale dryer, where the model exhibits an average error of 2% and 4% for moisture content and air temperature estimation, showing good fitting for practical data.

1. Introduction

The knowledge of the thermal properties is an essential tool used for many purposes, among which the analysis of heat transfers in complex systems, the choice of adequate insulating materials for energy-saving buildings and construction [1, 2], or the determination of the required energy to design equipment for the food industry [3].

Natural phosphates (NP) are the main source for phosphorus, an essential nutrient for plants and animals. They are used in various sectors, from the chemical industry to fertilizing along with biomedical [4]. The availability of these natural resources should ensure food security for developing countries and fulfill the global need for phosphate and its derivatives. Mined phosphates are found either as "mono-dicalcium phosphate," intended mainly for pet food manufacturing to enable animal growth, or "tricalcium phosphate," having the chemical formula $Ca_3(PO_4)_2$.

Phosphate mining goes through beneficiation operations to enhance product quality before being dried to meet export requirements in terms of moisture content. Such drying is performed using large rotary or flash dryers. To improve the energy efficiency and develop the operating and control strategy, users of flash dryers seek to evaluate process performances while targeting optimal operating conditions. For this purpose, several tools exist among which is the mathematical modeling that is considered as an effective tool for R&D costs and time savings. The model describes the transfer phenomenon occurring during drying, and its formulation requires the knowledge of the properties of the drying medium and particles to be dried. Up to now, the information regarding the thermophysical properties of

phosphate particles is scarce, thus the necessity for their investigation to analyze the performances of the flash dryer [5].

The determination of these thermal properties is generally carried out by means of two approaches: experimental measurement and/or modeling method [6]. The modeling approach requires a prior knowledge of the properties of the solid. This modeling approach is however not appropriate with the lack of information concerning the phosphate properties at the dry phase, such as the porosity and the geometry of the pore structure. Hence, the statistical modeling using the experimental approach is adopted.

Thermal conductivity is defined as the ratio of heat flux through a material to a temperature gradient (equation (1)). It describes the ability of the material to conduct heat. Two methods are used to experimentally establish the thermal conductivity: the steady-state technique and the transient method. The first is based on Fourier's first law, where a one-directional heat flux is applied through the sample. The drawback of this method is the long time required to reach equilibrium as the thermal conductivity is calculated for a constant gradient temperature. Among the steady-state techniques, there are the guarded hot plate and guarded heat flow [7]. On the contrary, the transient method is based on Fourier's second law and is widely used for the time gain it offers. Among the transient techniques, there are hot wire, hot plane, transient line source, and laser flash diffusivity [8].

$$\overrightarrow{\varphi} = -\lambda \overrightarrow{\text{grad}}\ (T). \tag{1}$$

Prior studies have identified the variables affecting the thermal conductivity of porous materials, such as temperature, pressure, moisture content, porosity, density, the geometry of the pore structure, and the geometrical distribution of the void and solid phases. These studies have adopted the experimental approach to characterize the thermal conductivity of a variety of products [9–17].

Considering the phosphate flash drying application, these variables will be limited to temperature, particle size and moisture content. In this sense, Bouguerra [1] used the transient line source method to investigate the effect of temperature and moisture content on the TC of wood-concrete mixtures. Experimental results showed that the thermal conductivity increased with temperature and moisture content. The same trend was observed by Xu et al. [18] when investigating the thermal conductivity dependence to temperature for lateritic clays. Jin et al. [6] investigated the thermal conductivity of sandy soils with porosity and moisture content variations. Experiments were conducted using both needle probe and hot plate methods, and results were used to model the thermal conductivity. They observed an increased thermal conductivity with increased moisture content, while a reduction was observed with porosity.

The second property of concern is the specific heat capacity, defined as the amount of heat required to increase the temperature of one gram of the material of a unit of temperature (equation (2)). The experimental determination of the specific heat can be achieved by two methods: direct and indirect. Indirect methods involve the knowledge of other properties of the material and can be less precise in their estimation. Among these methods are the flash method [19, 20] and technical MTPS [21, 22].

$$dQ = m \cdot C_{\text{p}} \cdot dT\,. \tag{2}$$

Direct methods rely on the use of calorimeters, such as adiabatic calorimeters [23], reaction calorimeters, or differential scanning calorimeters (DSC). The last technique is commonly used for the accuracy and ease of handling of the apparatus [24] while requiring only a small amount of the sample (few milligrams are enough). Several studies have used this technique to characterize the specific heat of various products, including foods [25–28], energy storage materials [29, 30], minerals [31], phase change material (PCM) [32], bentonite [33, 34], and quartz sand [35].

In this sense, Krupka et al. [31] measured the specific heat of different minerals (corundum, periclase, anorthite, muscovite, etc.), using the DSC technique in the temperature range 100–800°K. They observed a linearly increasing trend of the specific heat with temperature for all materials. The same trend was observed by Baumann and Zunft [35] when measuring the specific heat of quartz sand and sintered bauxite in the temperature range of 50–600°C. Toman and Černý [36] investigated the effect of the moisture content on the specific heat of high-performance concrete, ranging from dry matter to fully saturated, using a nonadiabatic calorimeter. They observed an increasing tendency of the specific heat with the moisture content.

This study targets the experimental investigation of the phosphate particles' thermal properties and performance analysis of phosphate particles' flash drying. In this regard, the thermal conductivity and specific heat capacity of phosphate particles are experimentally determined with moisture content, temperature, and particle size variation using the central composite design approach. The property experimental data are statistically modeled based on the response surface methodology (RSM) using Statgraphics Centurion software. The regression model developed for thermal properties is included in the flash drying model to analyze the thermal behavior and perform a validation of the model by comparison of the simulation results to the experimental data obtained for a flash dryer at bench scale.

2. Materials and Methods

2.1. Experimental Determination of the Phosphate Thermal Properties

2.1.1. Sample Preparation. Phosphate particles obtained from the phosphate ore are mainly composed of bone phosphate lime (BPL) and oxides of calcium and magnesium. The ore is valuable when containing a higher fraction

of BPL. The samples used for the experiments were sieved using an electronic siever Analysette 3, Fritsch [37], equipped with sieves r ranging from 40 μm to 300 μm. A duration of 20 minutes at 2 Hz was used for sieving the samples. The sieving results showed that the fraction of the sample having a mesh diameter less than 80 μm is 2%. This proportion was therefore neglected in the present study after 3 repeated tests showing the same results. The density of the sample is 1400 kg/m^3, measured using a water displacement method. The size distribution (Figure 1) was studied by sieve analysis considering particles as spheres.

Particles were initially dried at 130°C for 48 h in a convection oven until no mass variation was observed. Water was then added to reach the desired moisture content level. The phosphate particles and water were fully blended to reach an even water distribution. Moisture content of the samples was measured using Mettler Toledo Moisture Analyzer [38] at 200°C. Experiments were conducted at different moisture contents (1%–30%), temperatures (30–110°C), and particle sizes (100–300 μm).

2.1.2. Thermal Conductivity Measurement. Thermal conductivity (TC) was measured with a C-Therm TCi analyzer [39] which relies on the modified transient plane source method (MTPS). The setup (Figure 2) consists of a sensor connected to the control unit which converts the signal and transmits it to the computer. The sensor chip is made of 96% aluminum oxide coated with a thin sealing glass layer. The sensor operates by applying a one-directional heat flow to the sample. The sample absorbs a quantity of this heat, while the remaining results in a temperature rise of up to 3 K at the sensor surface [40]. The temperature rise is measured by recording the voltage drop at the sensor/sample interface. In fact, the sensor operates both as the heating source and as the voltage sensor.

Samples were filled in a 50 ml beaker until reaching a volume of 30 ml (following the supplier instructions). To ensure a better contact between the sensor and the sample, a 500 g weight was placed on the top of the sensor, enabling to compact better the sample and to avoid any heat exchange with the surrounding environment.

Calibration of the sensor was performed using three standards (distilled water, Pyrex, and Pyroceram), yielding results similar to manufacturer's values. The apparatus provides direct reading of the TC value based on the mean value of 10 measures.

2.1.3. Specific Heat Capacity Measurement. Specific heat capacity was measured using DSC Q20 (TA Instruments) with the modulated temperature option. Measurement by DSC was based on sample heating and calculation of the temperature difference between a reference (empty pan) and a sample. The experimental setup (Figure 3) consists of two sample holders (sample and reference) mounted inside a furnace, being heated radially. Two thermocouples are connected to each holder, while a thermoelement is connected between the two holders to measure the temperature difference measured as voltage [41].

Measurements were performed by placing 24.3 mg of the sample into a standard aluminum pan (40 μL) [42], which was then sealed hermetically. During measurement, the furnace was continuously purged with 60 mL/min of dry nitrogen gas to eliminate any water vapor. Specific heat capacities were calibrated with sapphire following the manufacturer's instructions [43], yielding to a calibration constant of 0.752. Specific heat was measured in the temperature range of 30 to 100°C at a linear heating rate of 3°C/min, with the modulation conditions of a 120-second period and ±1°C amplitude.

Specific heat of the phosphate particles was obtained as a direct output of the DSC apparatus, using TA Instruments Universal Analysis 2000 software.

2.1.4. Response Surface Methodology and Experimental Design. Experimental design is the best approach to obtain the maximum of information with the minimum number of tests. Several techniques are used to generate an experimental design, but the central composite design (CCD) remains the most widespread technique used to establish a second-order polynomial for the output function without having to resort to a full factorial design [44].

The response surface methodology (RSM) [45, 46] is a statistical approach that correlates several variables to a response function. It enables to test the effect of the variables and their interaction on the output while developing a mathematical model. Thus, the output function (Y) can be correlated to the variables (X_1, X_2, . . ., X_n) by means of the quadratic model:

$$Y = \beta_0 + \sum_{i=1}^{N} \beta_i X_i + \sum_{i=1}^{N} \beta_{ii} X_i^2 + \sum_{i \neq j}^{N} \beta_{ij} X_i X_j + \varepsilon, \quad (3)$$

with β_0, β_i, β_{ii}, and β_{ij} denoting the regression coefficients for the intercept, linear, quadratic, and interaction terms, respectively. ε represents the statistical error due to many sources, among which is the measurement error.

The validity of each of the preceding regression model is tested using the Fisher test, which compares the regression and experimental variances [47], with the rejection threshold set usually at 5%.

The factors and their limits considered for thermal conductivity and specific heat characterization are presented in Table 1.

2.2. Application of the Phosphate Characterization to the Flash Drying Analysis: Performance Model Development. In order to develop a performance model featuring a higher precision, the mathematical model of phosphate flash drying requires an accurate determination of the particle properties. The model is based on coupled transfers of heat, mass, and momentum between drying air and phosphate [5].

The thermal property regression results obtained from the experimental approach will be incorporated into the code of the flash dryer model using MATLAB software for its resolution. Simulation results are validated against experimental data obtained on a bench-scale solar flash dryer

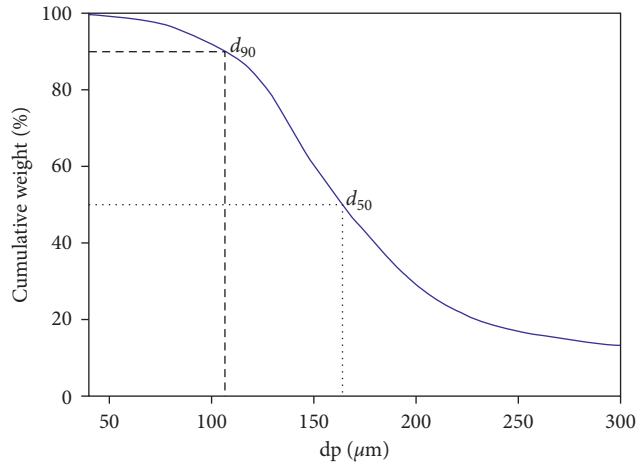

Figure 1: Particle size distribution.

Figure 2: C-Therm TCi apparatus for thermal conductivity measurement.

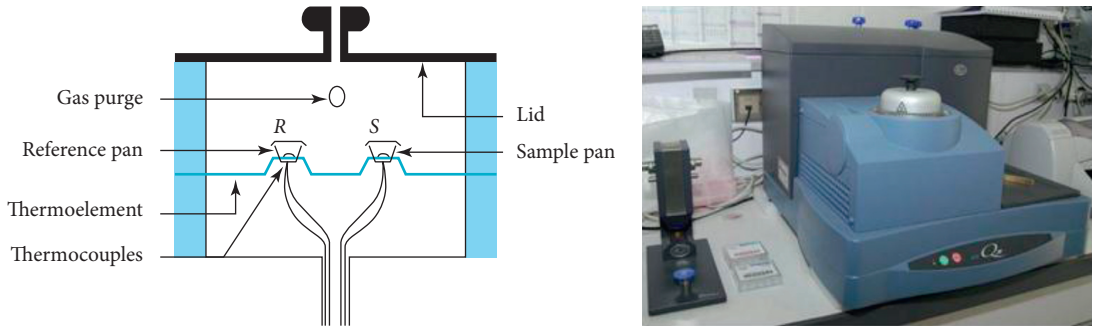

Figure 3: DSC apparatus for specific heat measurement. (a) Schematic diagram. (b) DSC Q20, TA Instruments.

Table 1: Factors and their limits for thermal conductivity and specific heat measurement.

Factor	Code	Unit	Limits	
			Min	Max
Particle diameter	X_1	μm	100	300
Moisture content	X_2	%	0.8	29.1
Temperature	X_3	°C	21	100

(1.7 m ∗ 200 mm internal diameter) as shown in Figure 2. The bench scale is coupled to a 29 kWth parabolic trough collector system [48] and installed at Green Energy Park (GEP-Ben Guerir).

The bench-scale flash dryer (Figure 4) consists of a drying chamber, air fan blower, a cyclone, and air filter, along with a draft fan responsible for the conveying of the drying air and phosphate particles along the dryer. Drying air was heated indirectly through a spiral crimped air-to-oil

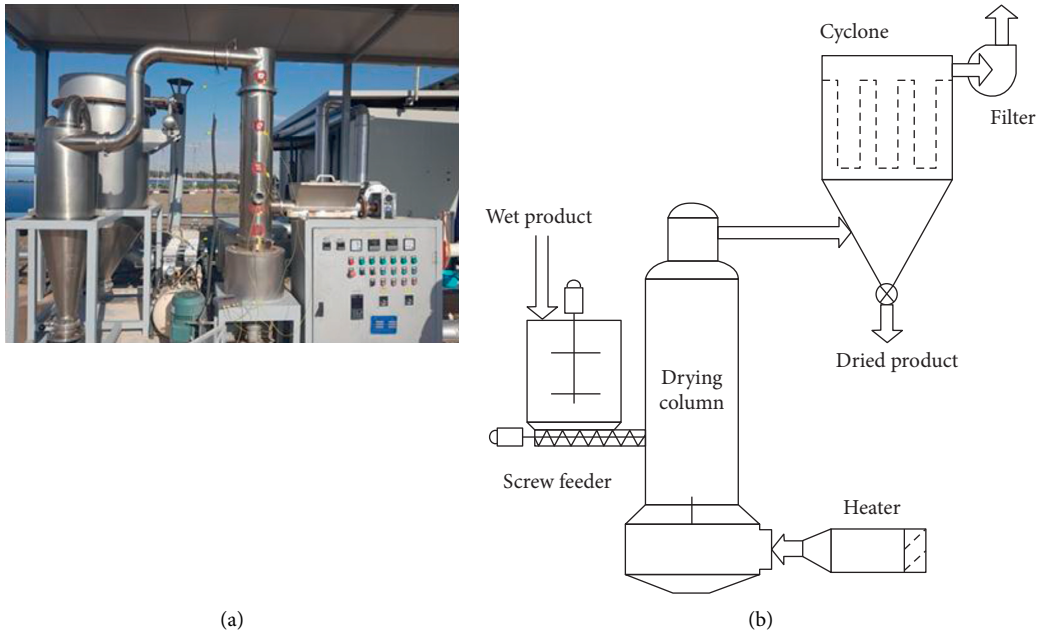

Figure 4: Bench-scale flash dryer. (a) Picture of the installed dryer. (b) Schematic diagram.

heat exchanger [49], yielding to a maximum air temperature of 126°C with an average air absolute humidity of 0.010 kg water/kg dry air.

The dryer was instrumented with thermocouples, which were inserted at five locations along the dryer length (0, 0.3, 0.7, 1.2, and 1.6 m), to measure the air temperature. A data acquisition system (OMEGA OMB-DAQ-2416) [50] was connected to the thermocouples to record the temperatures. Concerning the moisture content, the experimental tests will be limited to the initial and final moisture content.

3. Results and Discussion

3.1. Thermal Conductivity Statistical Modeling. The experimental variance was evaluated at the central point of the experimental design, corresponding to $d_p = 200\,\mu$m and MC = 15%, using 4 duplicate tests prepared in the same conditions. Results show a mean estimation of the thermal conductivity of 0.191 W/m K and a standard deviation of 0.0073. A coefficient of variation of 3.8% is found, corresponding to the standard error divided by the sample mean estimate.

The thermal conductivity values obtained through the experimental design are given in Table 2. A statistical analysis performed using Statgraphics Centurion software [51] yielded the regression coefficients and variance for each model. Table 3 summarizes the stepwise multiple linear regressions describing the experimental results which satisfy the Fisher test. A correlation not considering the temperature (equation (4)) is preferred as temperature is a perturbation variable in the present work, and its study field is limited.

$$k = 0.18 - 4.0\,10^{-4} d_p + 4.7\,10^{-4}\mathrm{MC}^2. \quad (4)$$

Figure 5 shows the response surface plot for the thermal conductivity of phosphate particles against particles' size and moisture content. Thermal conductivity increases with moisture content, which can be explained by the fact that adding water to the material leads to the air expulsion from the pores. As the air has low thermal capacity ($k_{air} = 0.028$ W/m·K) compared to water ($k_{water} = 0.664$ W/m·K), the pores filled with water are more conductive. Thus, the thermal conductivity is more important.

It can also be observed from Figure 5 that the thermal conductivity decreases with the particle size, a trend similar to other works [12, 52]. This phenomenon may be explained as follows: for solids with an important particle size, the volume of air filling the pores is greater, yielding to a decrease in the thermal conductivity since the presence of air in the pores adds an "insulation" character to the bulk sample.

3.2. Specific Heat Capacity Statistical Modeling. The experimental variance was evaluated through 3 repeated tests at the central point corresponding to a diameter of 200 μm with 17.9 mg ± 0.01 mg of particles in the temperature range 35–100°C. The results of repeated tests were evaluated at three different temperatures which enabled the calculation of the coefficient of variation, estimated to be 2%.

Table 4 presents the measured specific heat of phosphate particles (100, 200, and 300 μm) in the temperature range between 35 and 100°C. As shown in Figure 6, the specific heat capacity increases linearly with increasing temperature but decreases with particle diameter. Table 5 gives the regression coefficients correlating the specific heat capacity to temperature and particle diameter.

A more general model was fitted to correlate all experimental data of various particle diameters with

Table 2: Test results of the thermal conductivity with temperature as the perturbation variable.

No.	X_1	X_2	X_3	Thermal conductivity (W/m·K)
1	300	29	25.4	0.47
2	200	17	22.2	0.221
3	300	1.5	25	0.076
4	300	15.9	25	0.14
5	80	16.12	24.2	0.29
6	80	30.61	24.3	0.616
7	125	7.9	21.3	0.156
8	250	5.93	21.1	0.125
9	250	24.81	21.9	0.287
10	125	27.9	21.58	0.445
11	100	21.41	21.6	0.328
12	200	0.99	22.8	0.112
13	300	16.51	21.7	0.141
14	200	28.83	21.45	0.569
15	200	14.56	22.1	0.187

Table 3: Regression models for thermal conductivity tests.

Method	Stepwise multiple linear regressions	Variance (10^{-3})	ϑ_r	S_r^2/S_e^2	$F_{1-\alpha}(\vartheta_r, \vartheta_e)$
Forward stepwise multiple linear regression without constant	$k = 6\ 10^{-3} * T - 1.3\ 10^{-6} * {d_p}^2 + 4.7\ 10^{-4} * \mathrm{MC}^2$	1.49	12	0.202	8.763
Forward stepwise multiple linear regression with constant	$k = 0.18 - 4\ 10^{-4} * d_p + 4.7\ 10^{-4} * \mathrm{MC}^2$	1.68	12	0.210	8.763
Backward stepwise multiple linear regression without constant	$k = 3\ 10^{-4} * T^2 - 1.4\ 10^{-6} * {d_p}^2 + 4.7\ 10^{-4} * \mathrm{MC}^2$	1.52	12	0.206	8.763
Backward stepwise multiple linear regression with constant	$k = 0.14 - 1.2\ 10^{-6} * {d_p}^2 + 4.7\ 10^{-4} * \mathrm{MC}^2$	1.68	12	0.210	8.763

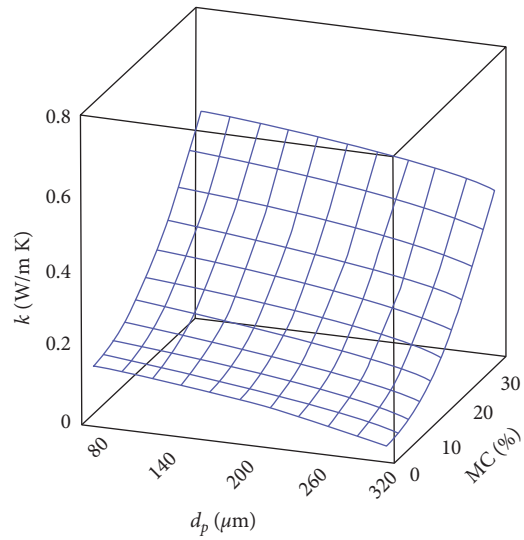

Figure 5: Response surface plot of the thermal conductivity vs. moisture content and particle size.

temperature variation. This yielded the following equation in the form

$$C_p = A(d_p) + B(d_p) * T, \quad (5)$$

with $A(d_p) = 0.511 - 1.49.10^{-9}{d_p}^3$ and $B(d_p) = 8.56.10^{-4} + 5.1.10^{-6}d_p - 1.49.10^{-8}{d_p}^2$.

The relative percentage deviation (RPD) was also calculated, estimated to a maximal value of 0.32%, indicating thus very good fitting of the experimental data.

As expected, the results show that the specific heat capacity increases with increasing temperature. This phenomenon may be explained as follows: as the temperature increases, more energy is supplied to bring the rotation and

Table 4: Experimental results of the specific heat capacity of phosphate particles.

Temperature (°C)	Specific heat capacity (J/g·°C)		
	100 μm	200 μm	300 μm
38	0.555	0.549	0.510
42	0.561	0.555	0.515
45	0.564	0.558	0.518
50	0.570	0.564	0.523
55	0.576	0.570	0.528
60	0.582	0.575	0.533
65	0.588	0.581	0.539
70	0.595	0.587	0.544
75	0.601	0.594	0.549
80	0.607	0.601	0.554
85	0.613	0.609	0.560
90	0.619	0.616	0.565
95	0.625	0.622	0.570
100	0.630	0.629	0.575

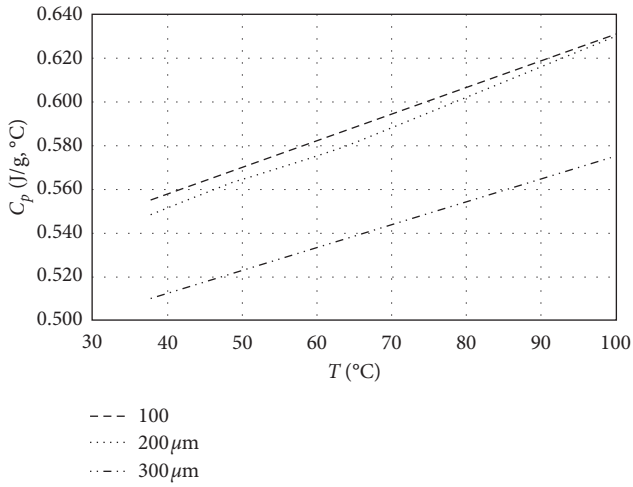

Figure 6: Effect of particle size and temperature on the specific heat of phosphate particles.

Table 5: Regression coefficients for the specific heat capacity.

Particle diameter (μm)	Regression coefficients				p value
	A	Standard deviation	B	Standard deviation	
100	0.509293	$4.51 * 10^{-4}$	$12.17 * 10^{-4}$	$6.3844E-06$	$p \leq 0.001$
200	0.49956	$1.30 * 10^{-3}$	$12.80 * 10^{-4}$	$1.846E-05$	$p \leq 0.001$
300	0.470696	$3.01 * 10^{-4}$	$10.45 * 10^{-4}$	$4.2634E-06$	$p \leq 0.001$

vibration of the molecules, yielding thus to the increase of their internal energy. As specific heat is defined as the slope of the internal energy plot with temperature, an increase in the internal energy implies thus an increase in the specific heat.

On the contrary, the specific heat decreases with increasing the particle size. This observation can be explained by the fact that heating larger particles requires more heat to generate the rotation of the atoms than smaller particles absorbing the same heat flow. The internal energy of the larger particles is thus less, implying a reduction in their specific heat capacity.

3.3. Flash Drying Analysis and Validation of the Performance Model. Thermal properties determined above were used to analyze the phenomenon occurring during phosphate particles' flash drying, showing that the phosphate particles exhibit a relatively low thermal conductivity which presents a poor thermal conductor. This fact explains the convective feature of flash drying, where moisture removal is governed by the convective transfers of free moisture at the surface of the particles, rather than the conduction inside the pores. The calculation of the thermal effusivity and diffusivity for phosphate particles from the present experimental data, at ambient temperature and dry state, yields to the following values: $D = 14.310^{-8}\ \mathrm{m^2/s}$ and $e = 291\ \mathrm{J/m^2 \cdot C \cdot s^{1/2}}$. As the thermal effusivity enables quantifying the ability of a material to change temperature when receiving a heat flow with a nonuniform distribution, two phenomena are combined: a heat flow is absorbed according to the specific heat capacity, and later, this heat flow is transferred to adjacent areas according to the thermal conductivity.

In order to validate the mathematical model, experimental tests were organized following an experimental design, where air temperature, phosphate mass flow rate, and product moisture content were varied in the range of 100–126°C, 45–72 kg/h, and 14–18%, respectively, as shown in Table 6. Particles collected from the cyclone after drying were analyzed using a moisture analyzer [38] to measure the final moisture content.

Simulations were performed with MATLAB using the fourth-order Runge–Kutta function to solve the model's equations. Detailed comparison of simulation results and experimental data is given for the test N°1, as shown in Figures 7 and 8. It can be noted in test N°1 that the measured moisture content at the dryer outlet is 0.76%, while the simulated moisture content is 0.78%, showing an error of 2.5%. On the contrary, the measured temperatures at different positions are 101.5, 81.26, 74.36, 68.2, and 63.25°C against simulations of 101, 79.6, 70.4, 64, and 60.6°C. Simulation results fall among the average error bars of ±2.2°C for the thermocouple. For this test, an average error of 3.6% is estimated for the temperature measurement, as shown in Table 7.

Subsequent test results are reported in Table 6. For all tests, the model average error for moisture content and temperature estimation is 2% and 4.5%, showing good fitting for practical purposes.

Considering the Biot number as an important parameter in conjugate heat and mass transfer, it was calculated in function of the model outputs. The calculation shows an

Table 6: Parameter variation for the experimental tests.

Test	Theoretical design variables			Experimental test variables			Moisture content (%)	
	T (°C)	Q_p (kg/h)	MC (%)	T (°C)	Q_p (kg/h)	MC (%)	Experimental	Simulations
1	100	60	14	101	100	10.36	0.76	0.78
2	110	71.82	16	115	72	16.49	0.76	0.77
3	120	45	17	125	60	17.45	0.61	0.62
4	110	55	14.31	100	45	14.65	0.94	0.97
5	100	40	14	98	39.15	12.71	0.77	0.78
6	120	65	17	115	51.84	14.87	0.77	0.78

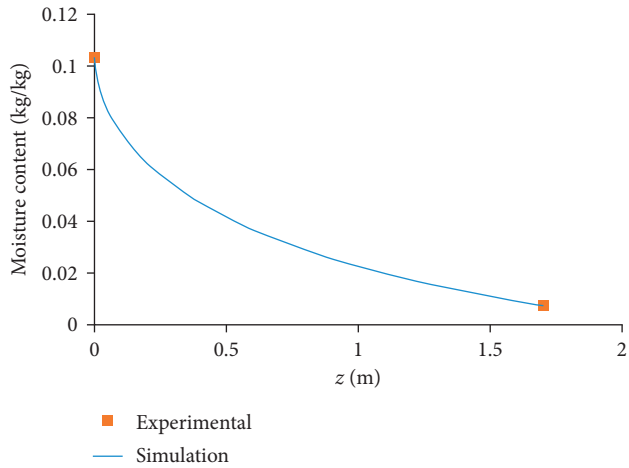

Figure 7: Moisture content profile along the dryer length: simulation vs. experimental.

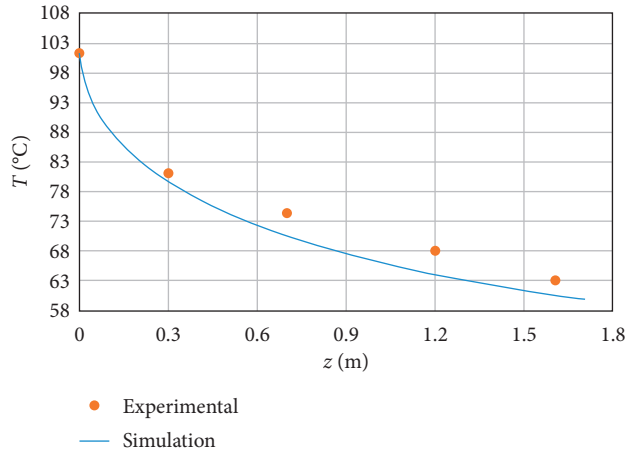

Figure 8: Temperature profile along the dryer length: simulation vs. experimental.

Table 7: Temperature error calculation for each position (test N°1).

Position	Corresponding dryer length (m)	Air temperature (°C)		Error calculation (%)
		Experimental	Simulated	
$Z1$	0	101.5	101	0
$Z2$	0.3	81.26	79.56	2
$Z3$	0.7	74.36	70.40	5
$Z4$	1.2	68.2	63.98	6
$Z5$	1.6	63.25	60.61	4

average value of 14 indicating a "thermally thick substance" [53], which is characterized by a slow heat conduction inside the material compared to heat convection at its surface. The obtained value confirms the analysis discussed above concerning the thermal behavior of phosphate particles along the flash dryer.

4. Conclusion

This paper presents the experimental characterization of thermal properties for phosphate particles for the performance analysis of the phosphate flash dryer. In this context, the thermal conductivity and specific heat capacity of phosphate particles were investigated through experimental measurements with moisture content, temperature, and particle size variation in the range 1–30%, 35–100°C, and 100–300 μm, respectively. These properties were studied through a response surface methodology.

The thermal conductivity was measured using the transient plane source method, while the specific heat capacity was measured using the DSC. The experimental results of the thermal properties were fitted using a multilinear regression. The developed correlations for the thermal properties were incorporated into the phosphate flash drying model. This model was simulated and compared to experimental data obtained in the present work. The main results are presented as follows:

Thermal conductivity increased with moisture content and temperature, showing good agreement with the literature results, while an inversional effect was observed with particle diameter

Regarding the specific heat capacity tendency, it increased linearly with temperature while decreased with increasing particle size

The regression models of the thermal properties were found statistically significant, having a relative percentage deviation of 3.8% and 0.32% for the thermal conductivity and specific heat capacity, respectively

Considering the results of the phosphate thermal properties, an analysis of the phenomenon occurring in the flash dryer showed that the particles exhibit a poor thermal conductor aspect, thus explaining the necessity to operate convective drying for surface moisture removal

Simulation results were compared with experimental data obtained on the bench-scale flash dryer, showing good agreement with a relative error of 2% and 4% for moisture content and drying air estimation; the validated model will be used in the future work to evaluate the performance of the industrial flash dryer and to design an industrial solar flash dryer

Nomenclature

A: Area (m^2)
C: Heat capacity (J/kg)
C_d: Drag coefficient
d_p: Particle diameter (m)
f: Frictional coefficient
g: Gravity acceleration (m/s^2)
G: Mass flow rate (kg/s)
k: Thermal conductivity (W/m K)
$K(\theta)$: Incidence angle modifier (IAM)
h: Convective heat transfer coefficient ($W/m^2 \cdot K$)
H: Air humidity (kg/kg)
L_v: latent heat of vaporization (J/kg)
MC: Moisture content (kg/kg)
P: Pressure (Pa)
Q: Heat (W)
T: Temperature (C)
V: Velocity (m/s)

Greek letters

ε: Volume fraction
ρ: Density (kg/m^3)

Subscripts

A: Air
P: Particle

Abbreviations

MC: Moisture content
TC: Thermal conductivity
ID: Internal diameter.

Data Availability

The experimental data used to support the findings of this study are included within the article.

Additional Points

Highlights. (i) Characterization of the thermal properties of phosphate particles: thermal conductivity and specific heat capacity; (ii) experimental approach using the modified transient plane source, differential scanning calorimetry, and experimental design; (iii) effect of temperature, moisture content, and particle size on the thermal properties; (iv) performance analysis of phosphate flash drying; and (v) validation of the developed phosphate flash drying model using own bench-scale tests.

Conflicts of Interest

The authors declare that they have no conflicts of interest.

Acknowledgments

This study was funded by IRESEN—Institut de Recherche en Energie Solaire et Energies Nouvelles (Grant INNOTHERM III S-FLASH).

References

[1] A. Bouguerra, "Temperature and moisture dependence on the thermal conductivity of wood–cement-based composite: experimental and theoretical analysis," *Journal of Physics D: Applied Physics*, vol. 32, no. 21, p. 2797, 1999.

[2] F. Batool, N. G. N. Prasad, and V. Bindiganavile, "Statistical modeling of thermal conductivity for cement-based foam," *Journal of Building Engineering*, vol. 19, pp. 449–458, 2018.

[3] B. Šeruga, S. Budžaki, Ž. Ugarčić-Hardi, and M. Šeruga, "Effect of temperature and composition on thermal conductivity of "Mlinci" dough," *Czech Journal of Food Science*, vol. 23, pp. 152–158, 2005.

[4] R. Z. Legeros, S. Lin, R. Rohanizadeh, D. Mijares, and J. P. Legeros, "Biphasic calcium phosphate bioceramics: preparation, properties and applications," *Journal of Materials Science: Materials in Medicine*, vol. 14, no. 3, pp. 201–209, 2003.

[5] Z. El Hallaoui, S. Vaudreuil, T. Moudakkar, and T. Bounahmidi, "One-dimensional phosphate flash dryer model for design application," *Drying Technology*, vol. 37, no. 2, pp. 139–148, 2019.

[6] H. Jin, Y. Wang, Q. Zheng, H. Liu, and E. Chadwick, "Experimental study and modelling of the thermal conductivity of sandy soils of different porosities and water contents," *Applied Sciences*, vol. 7, no. 2, p. 119, 2017.

[7] N. Yüksel, "The review of some commonly used methods and techniques to measure the thermal conductivity of insulation materials," *Insulation Materials in Context of Sustainability, Chapter 6*, IntechOpen Limited, London, UK, 2015.

[8] A. Palacios, L. Cong, M. E. Navarro, Y. Ding, and C. Barreneche, "Thermal conductivity measurement techniques for characterizing thermal energy storage materials—a review," *Renewable and Sustainable Energy Reviews*, vol. 108, pp. 32–52, 2019.

[9] S. Mo, P. Hu, J. Cao, Z. Chen, H. Fan, and F. Yu, "Effective thermal conductivity of moist porous sintered nickel material," *International Journal of Thermophysics*, vol. 27, no. 1, pp. 304–313, 2006.

[10] J. C. Géminard and H. Gayvallet, "Thermal conductivity of a partially wet granular material," *Physical Reviews E-Stat Physics, Plasmas, Fluids, Relat Interdiscip Top*, vol. 64, p. 5, 2001.

[11] A. C. Whaley, *Experimental Measurement of Thermal Conductivity of an Unknown Material*, Springer, Berlin, Germany, 2008.

[12] M. Wang, N. Pan, J. Wang, and S. Chen, "Mesoscopic simulations of phase distribution effects on the effective thermal conductivity of microgranular porous media," *Journal of Colloid and Interface Science*, vol. 311, no. 2, pp. 562–570, 2007.

[13] R. Askari, S. Taheri, and S. H. Hejazi, "Thermal conductivity of granular porous media: a pore scale modeling approach," *AIP Advances*, vol. 5, 2015.

[14] A. K. Mahapatra, Y. Lan, and D. L. Harris, "Influence of moisture content and temperature on thermal conductivity and thermal diffusivity of rice flours," *International Journal of Food Properties*, vol. 14, no. 3, pp. 675–683, 2011.

[15] A. N. Califano and A. Calvelo, "Thermal conductivity of potato between 50 and 100°C," *Journal of Food Science*, vol. 56, no. 2, pp. 586-587, 1991.

[16] I. N. Hamdhan and B. G. Clarke, "Determination of thermal conductivity of coarse and fine sand soils," *Procedure World Geotherm Congress*, vol. 44, no. 6, pp. 3969–3990, 2012.

[17] T. Nikiforova, M. Savytskyi, K. Limam, W. Bosschaerts, and R. Belarbi, "Methods and results of experimental researches of thermal conductivity of soils," *Energy Procedia*, vol. 42, pp. 775–783, 2013.

[18] Y. Xu, D. a. Sun, Z. Zeng, and H. Lv, "Effect of temperature on thermal conductivity of lateritic clays over a wide temperature range," *International Journal of Heat and Mass Transfer*, vol. 138, pp. 562–570, 2019.

[19] W. J. Parker, R. J. Jenkins, C. P. Butler, and G. L. Abbott, "Flash method of determining thermal diffusivity, heat capacity, and thermal conductivity," *Journal of Applied Physics*, vol. 32, no. 9, pp. 1679–1684, 1961.

[20] K. Shinzato and T. Baba, "A laser flash apparatus for thermal diffusivity and specific heat capacity measurements," *Journal of Thermal Analysis and Calorimetry*, vol. 64, no. 1, pp. 413–422, 2001.

[21] M. Pomianowski, P. Heiselberg, R. L. Jensen, R. Cheng, and Y. Zhang, "A new experimental method to determine specific heat capacity of inhomogeneous concrete material with incorporated microencapsulated-PCM," *Cement and Concrete Research*, vol. 55, pp. 22–34, 2014.

[22] A. Berge, B. Adl-Zarrabi, and C.-E. Hagentoft, "Determination of specific heat capacity by transient plane source," *Frontiers of Architectural Research*, vol. 2, no. 4, pp. 476–482, 2013.

[23] Q. Zhong, X. Dong, Y. Zhao et al., "Adiabatic calorimeter for isochoric specific heat capacity measurements and experimental data of compressed liquid R1234yf," *The Journal of Chemical Thermodynamics*, vol. 125, pp. 86–92, 2018.

[24] T. Kousksou, A. Jamil, Y. Zeraouli, and J.-P. Dumas, "Equilibrium liquidus temperatures of binary mixtures from differential scanning calorimetry," *Chemical Engineering Science*, vol. 62, no. 23, pp. 6516–6523, 2007.

[25] R. Y. Murphy, B. P. Marks, and J. A. Marcy, "Apparent specific heat of chicken breast patties and their constituent proteins by differential scanning calorimetry," *Journal of Food Science*, vol. 63, no. 1, pp. 88–91, 1998.

[26] A. I. Hobani and A. M. Elansari, "Effect of temperature and moisture content on thermal properties of four types of meat Part Two: specific heat & enthalpy," *International Journal of Food Properties*, vol. 11, no. 3, pp. 571–584, 2008.

[27] S. Heidenreich, T. Langner, and H. Rohm, "Heat capacity of cheese," *Journal of Thermal Analysis and Calorimetry*, vol. 89, no. 3, pp. 815–819, 2007.

[28] N. Wang and J. G. Brennan, "The influence of moisture content and temperature on the specific heat of potato measured by differential scanning calorimetry," *Journal of Food Engineering*, vol. 19, no. 3, pp. 303–310, 1993.

[29] G. Ferrer, C. Barreneche, A. Solé, I. Martorell, and L. F. Cabeza, "New proposed methodology for specific heat capacity determination of materials for thermal energy storage (TES) by DSC," *Journal of Energy Storage*, vol. 11, pp. 1–6, 2017.

[30] R. M. Saeed and J. P. Schlegel, "Uncertainty of thermal characterization of phase change," *Material by Differential Scanning Calorimetry Analysis*, vol. 5, pp. 405–412, 2016.

[31] K. Krupka, R. A. Robie, and B. S. Hemingway, "High-temperature heat capacities of corundum, periclase, anorthite, CaAl2Si2O8, glass, -muscovite, pyrophtllite, KAISi3O8 glass, grossular, and NaAlSi3O8 glass," *Am Mineral*, vol. 64, pp. 86–101, 1979.

[32] C. Barreneche, A. Solé, L. Miró, I. Martorell, A. I. Fernández, and L. F. Cabeza, "Study on differential scanning calorimetry analysis with two operation modes and organic and inorganic

phase change material (PCM)," *Thermochimica Acta*, vol. 553, pp. 23–26, 2013.
[33] L. M. Casás, J. L. Legido, M. Pozo, L. Mourelle, F. Plantier, and D. Bessières, "Specific heat of mixtures of bentonitic clay with sea water or distilled water for their use in thermotherapy," *Thermochimica Acta*, vol. 524, no. 1-2, pp. 68–73, 2011.
[34] S. Yoon, J.-S. Jeon, G.-Y. Kim, J.-H. Seong, and M.-H. Baik, "Specific heat capacity model for compacted bentonite buffer materials," *Annals of Nuclear Energy*, vol. 125, pp. 18–25, 2019.
[35] T. Baumann and S. Zunft, "Properties of granular materials as heat transfer and storage medium in CSP application," *Solar Energy Materials and Solar Cells*, vol. 143, pp. 38–47, 2015.
[36] J. Toman and R. Černý, "Temperature and moisture dependence of the specific heat of high performance concrete," *Acta Polytech*, vol. 41, pp. 6–8, 2001.
[37] Operating instructions VIBRATORY SIEVE SHAKER 2019, https://www.fritsch-international.com.
[38] Mettler Toledo Moisture Analyser Excellence Plus HX204 Operating Instructions. http://www.mt.com/. Operating Instructions Moisture Analyzer HR83 and HR83-p 2012:114.
[39] N. Wooden, *Operating Procedure for the TCI: Small Volume Test Kit for Thermal Conductivity Testing*, C-Therm Technologies, Amherst, Nova Scotia, Canada, 2008.
[40] S. Jayachandran, R. N. Prithiviraajan, and K. S. Reddy, "Characterization of various two-phase materials based on thermal conductivity using modified transient plane source method," *AIP Conference Proceedings*, vol. 1859, 2017.
[41] A. Boller, Y. Jin, and B. Wunderlich, "Heat capacity measurement by modulated DSC at constant temperature," *Journal of Thermal Analysis*, vol. 42, no. 2-3, pp. 307–330, 1994.
[42] Mettler Toledo MS204 Manuals M. and UG for M. T., Precision and Analytical Balances MS-TS.
[43] L. C. Thomas, *TA Instruments. Modulated DSC^{TM} Compendium, Basic Theory and Experimental Consider-Ations. TA-210. Modulated DSC® Basics; Optimization of MDSC® Experimental Conditions*, TA Instruments, Inc., New Castle, DE, USA, 2001.
[44] P. Sahoo and J. K. Barman, "ANN modelling of fractal dimension in machining," *Mechatronics Manufacturing Engineering Research Development*, vol. 159–226, 2012.
[45] D. Datta and S. Kumar, "Modeling using response surface methodology and optimization using differential evolution of reactive extraction of glycolic acid," *Chemical Engineering Communications*, vol. 202, no. 1, pp. 59–69, 2015.
[46] A. T. Nair, A. R. Makwana, and M. M. Ahammed, "The use of response surface methodology for modelling and analysis of water and wastewater treatment processes: a review," *Water Science and Technology*, vol. 69, no. 3, pp. 464–478, 2014.
[47] G. Tanase and J. G. S. M. Dobre, *Chemical Engineering: Modelling, Simulation and Similitude*, Weinheim Wiley-VCH 2007, Weinheim, Germany, 2007.
[48] T. Moudakkar, Z. El Hallaoui, S. Vaudreuil, and T. Bounahmidi, "Modeling and performance analysis of a PTC for industrial phosphate flash drying," *Energy*, vol. 166, pp. 1134–1148, 2019.
[49] T. Moudakkar, Z. El Hallaoui, S. Vaudreuil, and T. Bounahmidi, "Optimum design and performance analysis of heat exchanger coupling a flash dryer and parabolic trough collectors," *Solar Energy*, vol. 199, pp. 152–163, 2020.
[50] Operating Instuctions O. M. E. G. A., OMB-DAQ-2416 Series.
[51] Statgraphics 18 FREE VERSION, 2019, http://www.statgraphics.com/centurion-xvii.
[52] X. Ma, A. J. Peyton, and Y. Y. Zhao, "Measurement of the electrical conductivity of open-celled aluminium foam using non-contact eddy current techniques," *NDT & E International*, vol. 38, no. 5, pp. 359–367, 2005.
[53] M. Hatami, D. D. Ganji, and M. Sheikholeslami, *DTM for Particles Motion, Sedimentation, and Combustion*, Academic Press, Cambridge, MA, USA, 2017.